Projectile energy dependence of L x-ray emission from fast, highly charged Xe ions traveling in solids

V. Horvat, R. L. Watson, and J. M. Blackadar
Cyclotron Institute and Department of Chemistry, Texas A&M University, College Station, Texas 77843
(Received 7 February 1997)

L x-ray emission from Xe ions incident on a variety of solid targets at energies ranging from 6 to 15 MeV/u has been investigated using a curved crystal spectrometer of moderate resolution. Analysis of the spectra provided estimates of the average charges and (in some cases) the charge distributions of those ions emitting L x rays inside the targets. Calculations employing theoretical electron capture and loss cross sections were used to examine the dependence on depth within the target of contributions to the spectra from Xe ions having different average numbers of L and M electrons. Average charges and charge distributions deduced from the x-ray spectra were found to agree quite well with those predicted by the model calculations. [S1050-2947(97)00909-8]

PACS number(s): 34.50.Fa, 32.30.Rj

I. INTRODUCTION

The spectra of x rays emitted by fast ions as they traverse matter can provide information relating to the populations of states from which the x rays originate. Therefore, they are potentially useful sources of data for testing *ab initio* descriptions of the charge distributions of heavy ions slowing down in matter, which rely heavily on their ability to predict the average quantum state populations. Furthermore, if the x-ray emitting states dominate the distribution of states in existence after the ions have reached charge equilibrium, it may be possible to deduce the equilibrium charge distribution directly from the x-ray spectrum. The merit of such an approach is that it would provide a method for studying charge distributions of ions *inside* matter as opposed to simply observing the charge distributions existing after the ions have emerged into vacuum. The work described herein explores both of these possibilities.

In a preceding study [1], the spectra of L x rays emitted by 6- and 8-MeV/u Xe ions traveling in solid targets were measured and used to estimate the equilibrium charges of ions inside solids. The present paper reports on additional L x-ray spectral measurements which have been performed using 6-, 8-, 10-, and 15-MeV/u Xe ions incident on a variety of solid targets ranging in (average) atomic number from 3 to 18. This work was performed for the purpose of studying the evolution of the x-ray spectra with increasing number of L vacancies and to examine in detail the relationship between the average charges of ions contributing to the x-ray spectra and the average charges of all the ions. Model calculations of projectile L- and M-electron populations as a function of depth in the target have been used to provide a clearer understanding of thick-target x-ray spectra and to predict the average charges of contributing ions for comparison with those extracted from an analysis of the spectra. In a subsequent publication [2], these results for solid targets will be compared to those obtained in a similar set of measurements performed with gas targets.

II. EXPERIMENTAL METHODS

Beams of 6-, 8-, 10-, and 15-MeV/u Xe ions, with initial charges ranging from 17+ at 6 MeV/u to 25+ at 15 MeV/u, were extracted from the Texas A&M K-500 superconducting cyclotron, charge analyzed, and optically focused on a Zn/CdS phosphor with the aid of a closed-circuit television camera. The beam passed through a 2-mm-diameter collimator located directly in front of the target cell and a carbon foil of thickness 200 μg/cm^2 mounted between the collimator and the target cell. The carbon foil was used to monitor the beam current. Details concerning the spectrometer and the electronic apparatus are given in Refs. [1] and [3].

The targets consisted of the following: (a) thick ($\sim$2 mm) pressed pellets made from powders of pure C, NaF, and KCl, (b) a 0.25-mm-thick Be metal wafer, (c) a thick slice of Li metal, and (d) a 400-μg/cm^2 C foil. They were oriented at 45° with respect to the (horizontal) beam direction and at 45° with respect to the (vertical) spectrometer axis such that the spectrometer viewed them from the front. In some cases, a 2.1-mg/cm^2 Ni foil was placed over the entrance aperture of the target cell in order to produce beams with the same incident energies and charge distributions as those employed in subsequent measurements with gas targets where such Ni foils were used for gas cell windows. The energies (in units of MeV/u) of the projectiles after passing through the Ni foil were reduced to 5.2 (from 6), 7.2 (from 8), 9.3 (from 10), and 14.4 (from 15).

Energy calibration of the spectrometer was performed using the measured diffraction positions of the $K\alpha_{1,2}$ and $K\beta_1$ peaks of K, Ca, and Mn. The energy calibration was checked several times during the course of each cyclotron run.

III. QUALITATIVE FEATURES OF THE X-RAY SPECTRA

The wide variety of structural features displayed by the various spectra obtained in these measurements are illustrated by the compilations shown in Figs. 1 and 2. The Xe L x-ray spectra in Fig. 1, recorded using 14.4-MeV/u (energy after emerging from the Ni foil) Xe ions, demonstrate the dependence of the structure on (average) target atomic number, while the spectra in Fig. 2 show how the structure changes with incident projectile energy. Based on the previous study [1], these spectra are expected to contain primarily

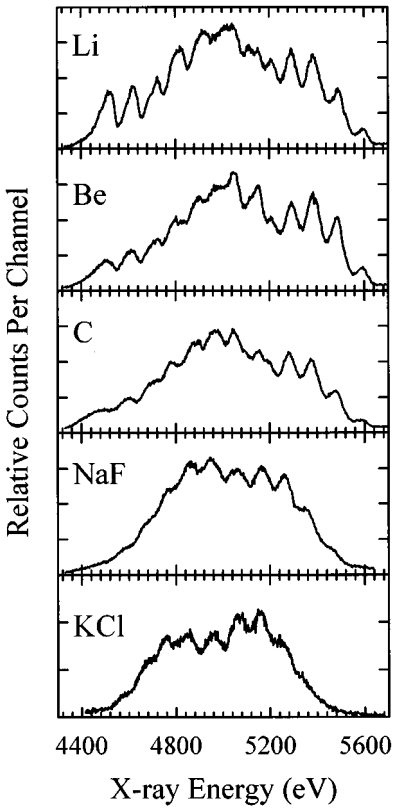

FIG. 1. Spectra of L x rays emitted by Xe ions traveling in thick solid targets of Li, Be, C, NaF, and KCl. The incident energy of the Xe ions is 14.4 MeV/u.

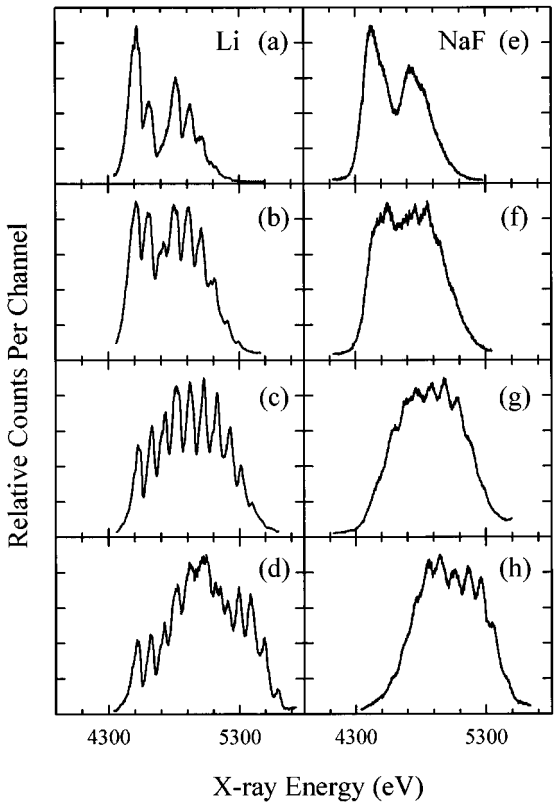

FIG. 2. Spectra of L x rays emitted by Xe ions traveling in solid Li [(a)–(d)] and solid NaF [(e)–(h)]. The incident energy of the Xe ions is 5.2 (a) and (e), 7.2 (b) and (f), 9.3 (c) and (g), and 14.4 MeV/u (d) and (h).

pairs of $L\alpha_{1,2}$ and $L\beta_1$ peaks arising from electron configurations containing one to eight L-shell vacancies. Each of these $L\alpha_{1,2}$ and $L\beta_1$ peak pairs will be shifted and broadened by multiple M-shell ionization, as well as by the Doppler effect. From the spectra taken at the higher incident projectile energies, it is evident that substantial contributions from $L\beta_3$ (and probably $L\beta_4$) lines also are present since the last peak at the high-energy end of the spectrum shown in Fig. 2(d) corresponds to the $L\beta_3$ peak in lithiumlike Xe.

In spite of the large variety of spectral shapes, some regularities can be noted. In Fig. 1, the most obvious trend is that the overall x-ray distribution width decreases as the (average) atomic number Z_2 of the target increases, which implies that contributions to the spectra from projectiles having the lowest and highest L-shell populations decrease with increasing Z_2. This observation is consistent with the fact that (a) the net rate of electron capture to the projectile L shell increase rapidly with Z_2, thereby causing the high-L-vacancy states to be quenched, and (b) x-ray-absorption coefficients increase rapidly with Z_2, thereby cutting off the detection of contributions from the low-L-vacancy states which are populated deep within the target after the projectile has lost much of its energy. In Fig. 2, it is evident that more peaks emerge at the high-energy end of the x-ray spectra as the projectile energy increases, while the relative intensities of the low-energy peaks decrease. This behavior reflects the fact that the net rate of the electron loss increases with projectile energy, resulting in higher average projectile charges, and the penetration depth also increases, resulting in higher absorption of the x rays from the lower charge states. Furthermore, the widths of the individual peaks are considerably greater in the spectra for the NaF target than in those for the Li target, indicating there is a larger variation in the number of M electrons attached to Xe projectiles traveling in NaF.

The energies corresponding to the individual peak centroids vary as a function of the initial projectile energy. However, this energy dependence does not appear to be systematic. For example, the first peak at the low-energy end of the spectra shown in Figs. 2(a)–2(d), corresponding to the case of Xe projectiles traveling in Li, shifts from 4523 eV at 5.2-MeV/u incident projectile energy down to 4516 eV at 7.2 MeV/u, then up to 4533 eV at 9.3 MeV/u and then down again to 4517 eV at 14.4 MeV/u. Another puzzling feature is the way the Li-induced Xe L x-ray spectrum evolves with projectile energy from 7.2 to 14.4 MeV/u, as shown in Figs. 2(b), 2(c), and 2(d). In particular, the spectrum at 9.3 MeV/u [Fig. 2(c)] looks much less complex (i.e., the peak positions are almost equidistant and the peak intensities vary smoothly) than the spectra at 7.2 and 14.4 MeV/u. In Fig. 2(d), the peaks around 5000 eV appear to be shifted and broadened relative to those appearing in Fig. 2(c), and they assume somewhat irregular shapes, although the widths of the individual peaks, in general, become smaller with increasing projectile energy. Some of the complexity in these spectra is associated with the fact that multiple M-shell ionization causes the peaks to shift to higher energies while the Doppler shift (at 90°) causes the peaks to shift to lower energies. Furthermore, the magnitudes of the shifts from both

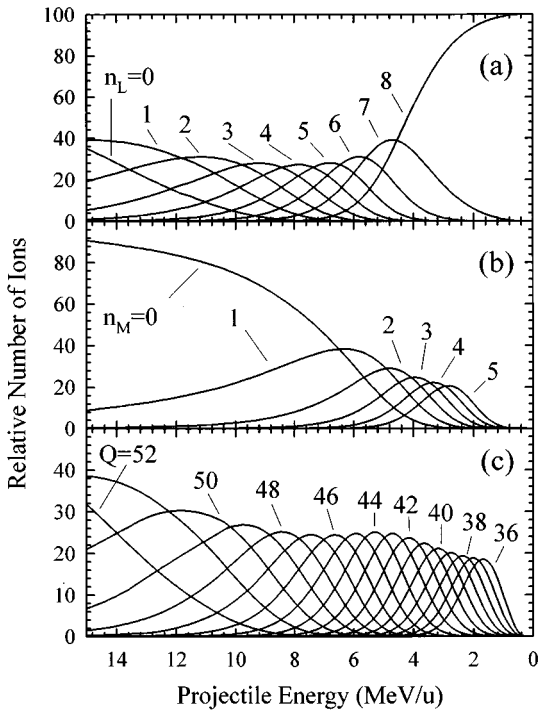

FIG. 3. Calculated dependence on projectile energy in a carbon target of the relative number of Xe ions having (a) the indicated number of L electrons, (b) the indicated number of M electrons, and (c) the indicated ionic charge.

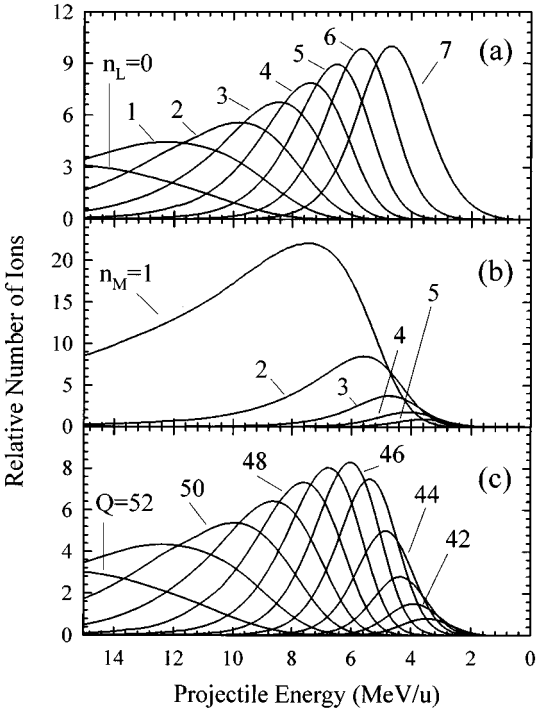

FIG. 4. Calculated dependence on projectile energy in a thick carbon target of the relative number of Xe ions that emit detectable L x rays and have (a) the indicated number of L electrons, (b) the indicated number of M electrons, and (c) the indicated ionic charge. The incident energy of the Xe ions is 15 MeV/u.

mechanisms vary with the depth of the projectile within the target.

IV. MODEL ANALYSIS OF PROJECTILE X-RAY EMISSION IN THICK TARGETS

The program ETACHA by Rozet, Stéphan, and Vernhet [4] was employed to gain insight into the composition of the Xe projectile L x-ray spectra obtained with thick targets. This program solves the rate equations for the population fractions (as a function of depth in the target) of all projectile configurations involving up to 28 electrons distributed over subshells having principal quantum numbers equal to 1, 2, and 3 using theoretical cross sections for electron capture, ionization, and excitation, and scaled radiative and Auger decay rates. The code was modified to incorporate Ziegler's method [5] of calculating the projectile energy loss, and to provide the additional output needed specifically for the purpose of this work.

The calculated equilibrium fractions of Xe ions having specific numbers of L and M electrons are shown in Figs. 3(a) and 3(b), respectively, as a function of the projectile energy in a carbon target. The corresponding charge distributions (calculated by assuming the K shells to be filled and all shells above the M shell to be empty) are shown in Fig. 3(c). These figures indicate that a 15-MeV/u Xe ion, upon entering a solid carbon target, becomes stripped of essentially all electrons above the L shell (on average) and retains only about one L electron (in addition to the two K electrons), resulting in an average charge of approximately 51. As the ion slows down in the target, its L- and M-shell populations steadily increase, and its average charge steadily decreases. By the time the ion has reached an energy of around 2 MeV/u, its L shell has become completely filled, at which point L x-ray emission is no longer possible.

To aid in the interpretation of the present x-ray spectra, it is useful to examine the relationship between the average charge of all ions and the average charge of ions that emit L x rays. In Figs. 4(a) and 4(b) we show the calculated fractions of Xe ions incident on a carbon target at an energy of 15 MeV/u that (i) have the specified numbers of L and M electrons and (ii) produce detectable L x rays as a function of the projectile energy in the target. They were obtained by excluding configurations having zero L vacancies and zero M electrons. In addition, they have been corrected for fluorescence yield (see the Appendix) and for absorption in the target [6] (which is why the x rays are referred to as ''detectable''). The curves in Fig. 4(c) show the corresponding charge distributions for ions that produce detectable L x rays. Comparing the curves in Fig. 4 with those in Fig. 3, it is evident that the relative contributions from individual configurations and charge states are quite different in the two cases. Nevertheless, the average charges computed from the two sets of curves in Figs. 3(c) and 4(c) are nearly the same, as is shown by the solid and dashed curves in Fig. 5. Over most of the energy range, the average charges of Xe ions emitting detectable L x rays deviate by less than one unit from the average charges of all the ions. At the high-energy end, the average charges of ions emitting detectable L x rays are slightly lower than the average charges of all ions because a large fraction of the ions have empty M shells and cannot emit L x rays. At the low-energy end, a large fraction

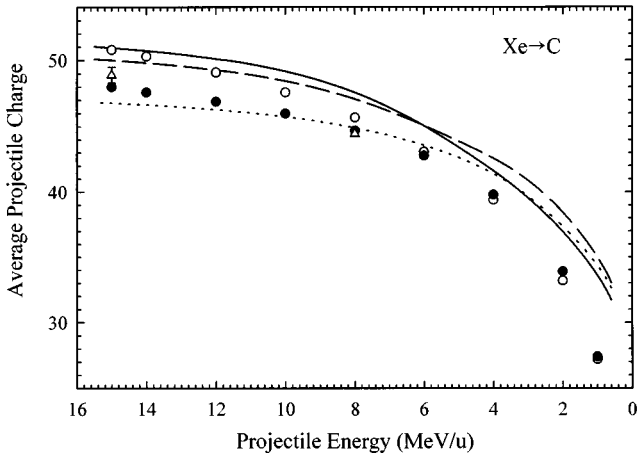

FIG. 5. Average charge of Xe ions in carbon as a function of projectile energy. The solid curve is the calculated average charge of all the Xe ions, the dashed curve is the calculated average charge of Xe ions that emit L x rays (i.e., of ions that contribute to thin-target x-ray spectra), and the dotted curve is the calculated average charge of Xe ions that contribute to thick-target x-ray spectra (as a function of *incident* projectile energy). Average equilibrium charges for Xe ions emerging from carbon foils are shown by the open triangles (measured by magnetic analysis [7]), the open circles (the semiempirical formula of Shima *et al.* [8]), and the filled circles (the semiempirical formula of Nikolaev and Dmitriev [9]).

of the ions have filled L shells and so the requirement of L x-ray detection automatically selects ions of higher-than-average charge. Also shown in Fig. 5 are (external) average equilibrium charges measured by magnetic analysis of 8- and 15-MeV/u Xe ions emerging from carbon foils [7], and those computed using the semiempirical formulas of Shima *et al.* [8] and Nikolaev and Dmitriev [9]. The experimental and semiempirical results lie somewhat below the average charges calculated with the ETACHA program (solid curve). At energies below 4 MeV/u, part of the discrepancy is undoubtably caused by the neglect of electrons occupying shells higher than the M shell in the model calculations. The measured thick-target x-ray spectra contain contributions from projectiles having the full range of energies in the target for which detectable L x rays are emitted. Therefore, in the case of carbon, where for an incident energy of 15 MeV/u this energy range extends all the way down to approximately 2 MeV/u (see Fig. 4), the average charge of ions contributing to the x-ray spectrum must be computed from the relative total x-ray yields of each contributing charge state. The relative total x-ray yields were determined from the relation [10]

$$Y_Q = \int_0^{E_i} \frac{N_Q(E)}{vS(E)}\, dE, \tag{1}$$

where E_i is the incident projectile energy, v is the projectile velocity, S is the stopping power, and N_Q is the relative number of ions having charge Q that emit detectable x rays [given for a carbon target by the curves in Fig. 4(c)]. The predicted average charge of ions contributing to (thick-target) x-ray spectra as a function of the *incident* projectile energy is shown by the dotted curve in Fig. 5. For Xe projectiles incident on a thick carbon target at an energy of 15 MeV/u, the predicted average charge of ions contributing to the thick-target L x-ray spectrum is approximately four units lower than the predicted average charge of all 15-MeV/u Xe ions traveling in carbon.

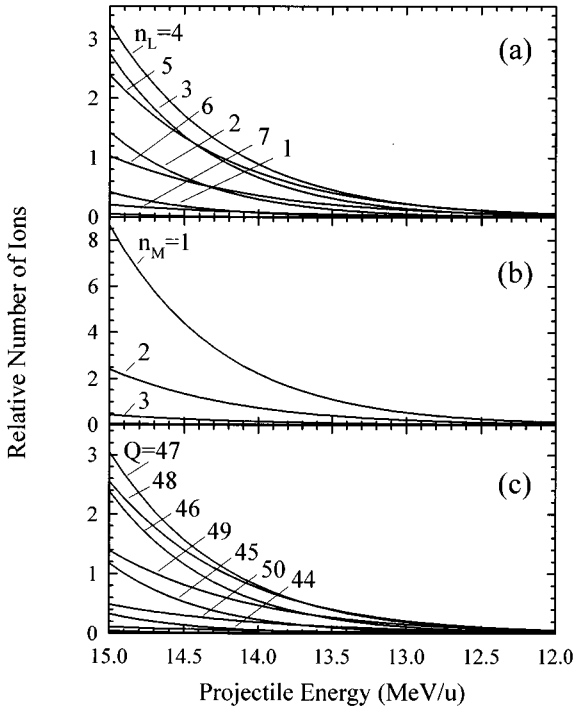

FIG. 6. Calculated dependence on projectile energy in a thick KCl target of the relative number of Xe ions that emit detectable L x rays and have (a) the indicated number of L electrons, (b) the indicated number of M electrons, and (c) the indicated ionic charge. The incident energy of the Xe ions is 15 MeV/u.

The situation is quite different for the KCl target because x-ray absorption in the target greatly limits the depth from which L x rays can be detected. This fact is illustrated in Fig. 6, where curves for a KCl target, corresponding to those for a carbon target in Fig. 4, are shown. In contrast to the wide range of projectile energies that contribute to the spectrum of L x rays emanating from a thick carbon target, the relevant energy range for L x-ray detection from a thick KCl target is quite narrow. This results in a much closer correspondence between the predicted average charges of all ions, of ions emitting detectable L x rays, and of ions contributing to the thick-target x-ray spectrum, as may be seen by referring to Fig. 7.

V. ANALYSIS OF THE X-RAY SPECTRA

A. Fitting procedure

In spite of their diversity, all of the collected Xe projectile L x-ray spectra were analyzed using a single fitting function which was developed as a generalization of the fitting function used in the previous study [1]. New features are the inclusion of $L\beta_3$ and $L\beta_4$ peaks, the removal of restrictions on relative intensities of components corresponding to a given L-shell occupation number, and independent determination of the average number of M electrons in the initial

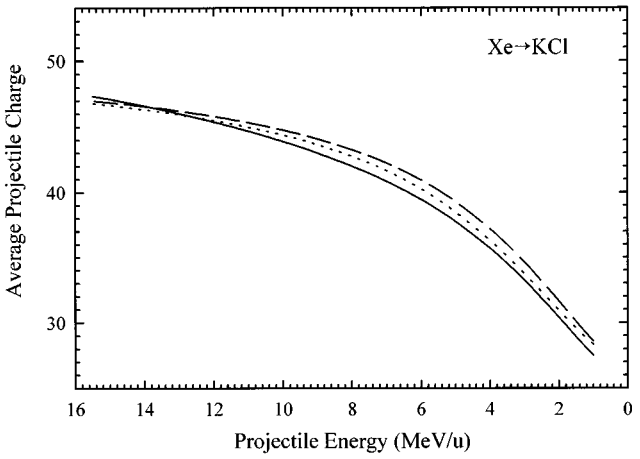

FIG. 7. Average charge of Xe ions in KCl as a function of projectile energy. The solid curve is the calculated average charge of all the Xe ions, the dashed curve is the calculated average charge of Xe ions that emit L x rays (i.e., of ions that contribute to thin-target x-ray spectra), and the dotted curve is the calculated average charge of Xe ions that contribute to thick-target x-ray spectra (as a function of *incident* projectile energy).

state for each component. Additionally, the method of calculating the relevant fluorescence yields (see the Appendix) was improved, and a linear term was introduced in the description of the background.

The variable parameters of the fitting function were the amplitudes $A(n_L)$ of the components corresponding to the L-shell population numbers n_L, the average number of M electrons for each component $\overline{n_M}(n_L)$, the standard deviation of individual x-ray peaks σ_x, two linear background parameters (the slope and intercept), and the set of relative intensity parameters $R(n_c)$ which can be regarded as corrections for non-statistical population of the L and/or M shell, as well as for the omission of other x-ray components. The index n_c specifies the transition type (e.g., $L\alpha, L\beta_1$, etc.). The maximum number of variable parameters was 23, while the maximum number of peaks considered was 126.

B. Calculation of the transition energies

The transition energies for the various initial L-shell configurations of Xe ions having a single M electron were calculated using the multiconfigurational Dirac-Fock program of Desclaux [11] by taking the differences between the average total energies of the initial and final configurations. However, it was found that some of the calculated transition energies for neonlike Xe deviated by as much as 30 eV from those obtained experimentally by Beiersdorfer *et al.* [12]. Therefore, correction factors having values of 1.0060, 1.0025, 0.9991, and 0.9992 (as determined from this comparison) for $L\alpha_1$, $L\beta_1$, $L\beta_3$, and $L\beta_4$ transitions, respectively, were applied to the corresponding calculated transition energies for all L-shell configurations. Finally, these corrected energies were scaled using the procedure described in Ref. [1] to obtain transition energies for ions having more than one M electron.

The Doppler shift of a 5000-eV x ray detected at an observation angle of 90° ranges from -32 eV at a projectile energy of 6 MeV/u to -79 eV at 15 MeV/u. Therefore, corrections for the Doppler shift had to be applied to the calculated transition energies. As is evident from the model analysis presented in Sec. IV, calculation of the average Doppler shift is a difficult problem when thick solid targets of low atomic number are used since in this case the detected x rays originate from a wide range of projectile energies. As the projectile penetrates a thick solid target, both its energy and its equilibrium electronic configuration continuously change. This means that ions with different numbers of L electrons will have different average velocities. A reasonably good determination of the average Doppler shift is very important in the present work since its value directly affects the average number of M electrons derived in the fitting procedure. The quality of the fit is affected as well, since the M-shell population distribution is assumed to be binomial, and therefore its width (standard deviation) is equal to its centroid. The average Doppler shift of L x rays emitted by projectiles having a given number of L electrons was calculated from the corresponding average projectile energy $\overline{E}$, which in turn was determined from N_{n_L}, the relative number of ions having n_L L electrons that emit detectable x rays [shown for a carbon target in Fig. 4(a)] by using the relation [10]

$$\overline{E}=\frac{\int_0^{E_i} E N_x(E)\,dE}{\int_0^{E_i} N_x(E)\,dE}, \tag{2}$$

where $N_x(E)=[N_{n_L}(E)/vS(E)]$.

C. Quantities derived from the fitting parameters

The average numbers of projectile L and M electrons were determined from the best-fit values of the amplitudes $A(n_L)$ using the relationships

$$\overline{n_{L \text{ or } M}}=\sum_{n_L=0}^{7}\sum_{n_M=1}^{18} n_{L \text{ or } M} \times Y(n_L,n_M) \Big/ \sum_{n_L=0}^{7}\sum_{n_M=1}^{18} Y(n_L,n_M), \tag{3}$$

where

$$Y(n_L,n_M)=\binom{18}{n_M} p_M^{n_M}(1-p_M)^{18-n_M}\frac{A(n_L)}{\sum_{n_L=0}^{7} A(n_L)}, \tag{4}$$

and the binomial probability p_M is equal to $\overline{n_M}/18$. The average projectile charge was calculated from the relationship

$$\overline{Q}=\sum_{Q=27}^{51} QY(Q), \tag{5}$$

where the charge yield fractions $Y(Q)$ were calculated by summing the $Y(n_L,n_M)$ over all combinations for which $n_L+n_M=52-Q$. The charge distribution widths σ_Q were calculated using the relation

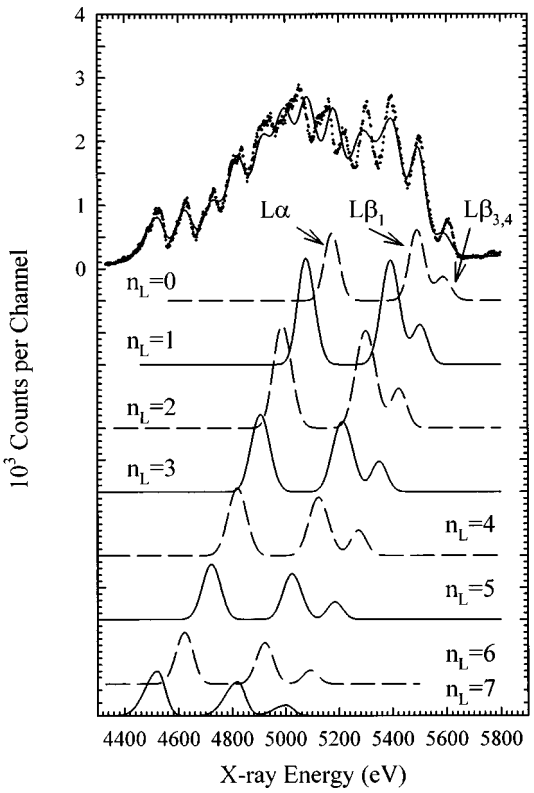

FIG. 8. Fitted spectrum of L x rays emitted by 15-MeV/u (incident energy) Xe ions traveling in lithium. The data points are shown as filled circles, while the fitted spectrum and its components (corresponding to the indicated L-shell population numbers) are shown by the solid and dashed lines.

$$\sigma_Q = \left[\sum_{Q=27}^{51} (Q-\overline{Q})^2 Y(Q) \right]^{1/2} . \qquad (6)$$

VI. RESULTS AND DISCUSSION

A. Quality of the fits

The most difficult of all the Xe L x-ray spectra to fit was the one obtained with 15-MeV/u Xe ions incident on a Li target, and it is shown in Fig. 8. The insets in this figure show the relative intensities of the x-ray components summed over all configurations having the specified numbers of L electrons. It should be emphasized that this spectrum contains contributions from projectiles spanning a very wide range of energies (15 to approximately 2 MeV/u) because the x-ray attenuation coefficients for Li are quite small. Furthermore, over this energy range, the L shells of the projectiles undergo transformation from fully stripped to completely filled. Considering the complications associated with the analysis of this spectrum, the fit reproduces the observed structure reasonably well and, in doing so, provides a measure of confidence in the procedures used to correct for the Doppler shift. Nevertheless, it must be admitted that the structure in the region of the spectrum from 4960 to 5260 eV is rather poorly represented and at least one component of the measured spectrum appears to be missing from the fitting function.

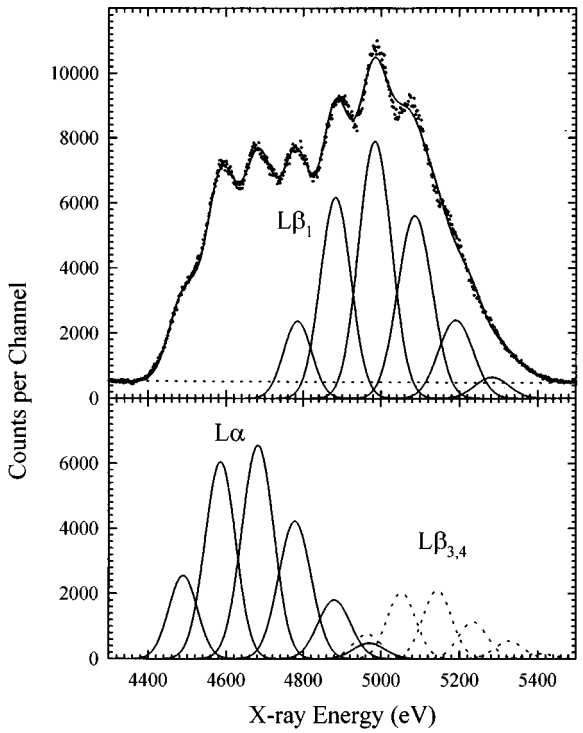

FIG. 9. Fitted spectrum of L x rays emitted by 9.3-MeV/u (incident energy) Xe ions traveling in KCl. The data points are shown as filled circles, while the fitted spectrum and its components are shown by the solid and dotted lines.

The fits obtained for the spectra of L x rays from Xe ions incident on the KCl target were quite good, as is illustrated in Fig. 9. As noted earlier, Xe L x rays are strongly absorbed in KCl, and hence these spectra are essentially thin-target spectra from projectiles having a narrow range of energies. The quality of the fits to the spectra obtained with all the other targets was similar to that shown in Fig. 9. Even the spectra obtained with the thick carbon target, which contained contributions from nearly the full range of projectile energies inside the target, were quite well reproduced by the fitting function.

The spectra measured previously at 6 and 8 MeV/u [1] were reanalyzed, and the overall quality of the fits obtained with the present analysis procedure was found to be slightly better than before. The best-fit values of the parameters from the two analyses were consistent with each other, aside from small differences ascribed to the following. (a) The previous procedure required the fractions of ions having different numbers of L electrons to be Gaussian and used this distribution to include the fraction with zero L vacancies in the calculation of the average number of L electrons per ion. The new procedure, in which the individual L-electron population fractions were allowed to vary independently, did not include the zero L-vacancy fraction in the calculation of the average number of L electrons per ion, which caused $\overline{n_L}$ to decrease (on average) by 0.5 electrons. (b) The previous procedure did not incorporate corrections for the Doppler shift, which caused the average number of M electrons per ion obtained in the previous analysis to be higher (on average) by one electron than those obtained in the present analysis.

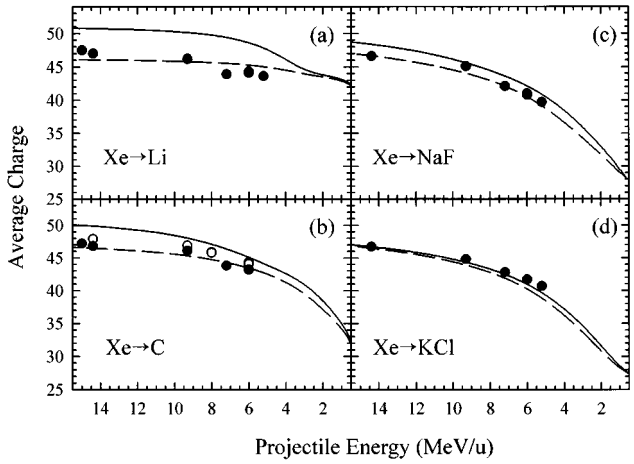

FIG. 10. Comparison of the average charges determined from the thick-target (filled circles) and thin-target (open circles) Xe L x-ray spectra with those predicted by the model calculations. The solid curves show the calculated average charges for thin targets, and the dashed curves show those for thick targets.

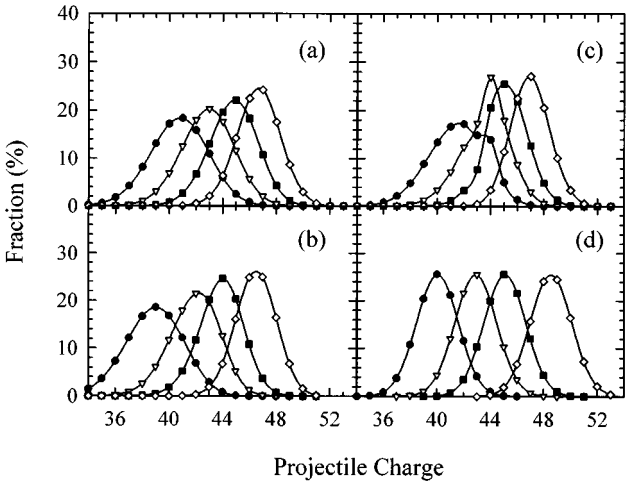

FIG. 11. Charge distributions (a) determined from thick-target x-ray spectra for Xe ions inside KCl, (b) calculated using the ETACHA program, (c) calculated from the distributions in (a) for Xe ions after emerging from KCl, and (d) predicted for Xe ions after emerging from KCl using semiempirical formulas [13,14]. The projectile energies (in MeV/u) are 4.8 (filled circles), 6.7 (open triangles), 8.7 (filled squares), and 13.7 (open diamonds).

B. Average charges

The average charges of ions contributing to the x-ray spectra, as determined from the fitting analyses, are compared with those predicted using the ETACHA population fractions in Fig. 10. The dashed curves show the average charges expected for Xe ions that contribute to thick-target L x-ray spectra as a function of incident projectile energy. The solid curves show the average charges expected for Xe ions that emit detectable L x rays as a function of projectile energy. (In other words, the solid curves show the average charges of Xe ions that would be expected to contribute to *thin*-target L x-ray spectra.) These curves were calculated as described in Sec. IV [e.g., the solid and dashed curves for carbon targets, in Fig. 10(b) are the same as the dashed and dotted curves, respectively, in Fig. 5].

Overall, it may be concluded that the values of the average charges deduced from the thick-target x-ray spectra and their dependence on projectile energy agree quite favorably with those predicted by the model calculations. At the high-energy end, the average charges of ions contributing to the thick-target spectra are very nearly the same for all the targets. As the incident projectile energy decreases, the average charge also decreases, but at a rate that increases with target atomic number, in agreement with the predictions.

Also contained in Fig. 10(b) are average charges deduced from Xe L x-ray spectra obtained with thin carbon targets. It is evident that these data points are somewhat lower than the average charges predicted by the model calculations for thin targets (solid line).

C. Charge distributions

According to the model calculations, the average charges of ions contributing to Xe L x-ray spectra obtained with a thick KCl target should be essentially the same as the average equilibrium charges of all ions (see Fig. 7). Therefore, it is worthwhile to examine the charge distributions determined from these x-ray spectra, which are shown in Fig. 11. The charge distributions in Fig. 11(a) are for ions traveling *inside* the target at the average energies indicated in the figure caption. The charge distributions shown in Fig. 11(c) are for ions having the same average energies after emerging from the target and undergoing deexcitation *outside* the target. These latter distributions were computed from the former by apportioning the yield of each electron configuration between its Auger and x-ray decay branches at each step of the deexcitation process until its final configuration (either a filled L shell or an empty M shell) was reached. In Fig. 11(b) are shown the charge distributions predicted by the ETACHA program for comparison with the x-ray results in Fig. 11(a), and in Fig. 11(d) are shown charge distributions calculated using the semiempirical formulation of Shima and coworkers [13,14] for comparison with those in Fig. 11(c).

The shapes of the (''interior'') charge distributions in Fig. 11(a) are almost Gaussian in most cases. This result is not inherent in the method of analysis since the distribution of the number of projectile M electrons was assumed to be binomial, but the contributions from projectiles having different numbers of L electrons were determined independently. The kink that appears in the deduced (''exterior'') charge distributions in Fig. 11(c) at charge 44 is a consequence of the nature of the relaxation process applied to the symmetrical interior charge distributions. That is, the relaxation is complete when either the L shell becomes filled or the M shell becomes empty. Ions that satisfy both criteria have a charge of 44, which corresponds to the location of the kink. The part of the charge distribution above 44 is mostly determined by the original L-shell population distribution, while the part of the charge distribution below 44 is mostly determined by the original M-shell population distribution. The kink arises when the widths of these two distributions are not the same. Relaxation outside the target does not change the average charges very much, as is evident from a comparison of the centroids of the corresponding distributions in Figs. 11(a) and 11(c). (The average ''exterior''

charge is greater than the average ''interior'' charge by 0.9 units at 6 MeV/u and by 0.3 units at 15 MeV/u.) The reason for this is that the M shell is highly depleted at these energies, and therefore the number of Auger decays is highly restricted.

The shapes and widths of the ETACHA charge distributions are in good agreement with those exhibited by the charge distributions deduced from the x-ray spectra, but the centroids of the former increasingly deviate toward lower average charges relative to those of the latter as the projectile energy decreases. In comparing Figs. 11(c) and 11(d), it may be seen that the centroid of the semiempirical distribution at the lowest projectile energy is 1.5 units lower than the centroid of the corresponding ''exterior'' charge distribution deduced from the x-ray spectra, while that for the highest energy is 1.6 units higher. Also, the ''x-ray'' charge distributions are somewhat broader than the semiempirical charge distributions, especially at the lower projectile energies. It should be noted, however, that the reliability of the semiempirical distributions at energies above 6 MeV/u has not yet been established.

VII. CONCLUSION

In general, the observed x-ray structure was consistent with that expected for Xe ions containing variable numbers of L and M electrons, although a few anomalous features appeared in the spectra obtained using a thick lithium target. The fitting procedure developed for the analysis of these spectra enabled the identification of individual $L\alpha$, $L\beta_1$, $L\beta_3$, and $L\beta_4$ lines for Xe ions having one to eight L-shell vacancies. The average numbers of M electrons were determined from the peak positions and widths.

Model calculations employing L- and M-shell population fractions obtained from the ETACHA program provided a clear view of how the average numbers of L and M electrons attached to the projectile evolve as a function of depth in the target. They also made it possible to examine the relationship between the average charges of Xe ions contributing to both thick- and thin-target L x-ray spectra and the average charges of all ions traveling in the target. For highly transparent targets of low Z_2 (such as lithium and carbon), the average charge of all the ions was predicted to be as much as six units higher at 15 MeV/u than the average charge of ions contributing to the thick-target x-ray spectrum. This difference was found to decrease both with decreasing projectile energy and with increasing target (average) atomic number. Because of the critical role x-ray absorption plays in limiting the range of projectile energies (in the target) that contribute to the x-ray spectrum, relatively high-Z_2 targets (such as KCl) yield spectra that are essentially independent of thickness.

The average charges of Xe ions contributing to the L x-ray spectra obtained with thick Li, C, NaF, and KCl targets were determined from the fitting analyses and found to be in good agreement with those predicted by the model calculations. The charge distributions for Xe ions traveling in a KCl target, deduced from the x-ray spectra, were examined and used to compute the corresponding charge distributions expected for ions that had exited the target and decayed to their ground states. Although the shapes and widths of the ''interior'' and ''exterior'' charge distributions were noticeably different, the average charges (centroids) deviated by less than one unit.

ACKNOWLEDGMENTS

We thank J. P. Rozet for providing a copy of the ETACHA program and instructing us in its use. This work was supported by the Robert A. Welch Foundation.

APPENDIX: CALCULATION OF THE FLUORESCENCE YIELDS

The average fluorescence yields $\omega[n_c,n_{L_1},n_{L_2},n_{L_3},\overline{n_M}(n_L)]$ were calculated from the line fluorescence yields $\Omega(n_c,n_{L_1},n_{L_2},n_{L_3},n_{M_1},n_{M_2},n_{M_3},n_{M_4},n_{M_5})$ using the following expressions:

$$\omega[n_c,n_{L_1},n_{L_2},n_{L_3},\overline{n_M}(n_L)]=\sum_{n_M=1}^{18}\omega(n_c,n_{L_1},n_{L_2},n_{L_3},n_M)\times\binom{18}{n_M}p_M^{n_M}(1-p_M)^{18-n_M}, \tag{A1}$$

where

$$\omega(n_c,n_{L_1},n_{L_2},n_{L_3},n_M)=\sum_{n_{M_1}=0}^{2}\sum_{n_{M_2}=0}^{2}\sum_{n_{M_3}=0}^{4}\sum_{n_{M_4}=0}^{4}\sum_{n_{M_5}=0}^{6}\delta_{n_M,n_{M_1}+n_{M_2}+n_{M_3}+n_{M_4}+n_{M_5}}(1-\delta_{n_{L_f}(n_c),2j_f(n_c)+1})\times(1-\delta_{n_{M_i}(n_c),0})P_{n_M}(n_{M_1},n_{M_2},n_{M_3},n_{M_4},n_{M_5})\Omega(n_c,n_{L_1},n_{L_2},n_{L_3},n_{M_1},n_{M_2},n_{M_3},n_{M_4},n_{M_5}) \tag{A2}$$

and

$$P_{n_M}(n_{M_1},n_{M_2},n_{M_3},n_{M_4},n_{M_5})=\frac{\binom{2}{n_{M_1}}\binom{2}{n_{M_2}}\binom{4}{n_{M_3}}\binom{4}{n_{M_4}}\binom{6}{n_{M_5}}}{\binom{8}{n_M}}. \tag{A3}$$

$n_{M_j}(n_c)$ $(j=1,2,3,4,5)$ is the initial number of electrons in the subshell M_j containing the active electron for transition n_c, $n_{L_f}(n_c)$ is the initial number of electrons in the subshell L_f containing the active vacancy for the transition n_c, and $j_f(n_c)$ is the total angular momentum quantum number of the active L-shell vacancy for the transition n_c. The Kronecker delta symbols δ in Eq. (A2) ensure that for each n_c, only the configurations with at least one M-shell electron and at least one L-shell vacancy in the appropriate subshells contribute to the sum. The factor P_{n_M} represents the relative statistical probability that a projectile having n_M electrons in the initial state assumes the specified subshell population. The line fluorescence yield is defined by the expression

$$\Omega(n_c,n_{L_1},n_{L_2},n_{L_3},n_{M_1},n_{M_2},n_{M_3},n_{M_4},n_{M_5}) = \frac{\Gamma^{n_c}(n_{L_1},n_{L_2},n_{L_3},n_{M_1},n_{M_2},n_{M_3},n_{M_4},n_{M_5})}{\Gamma^{\mathrm{tot}(X)}(n_{L_1},n_{L_2},n_{L_3},n_{M_1},n_{M_2},n_{M_3},n_{M_4},n_{M_5})+\Gamma^{\mathrm{tot}(A)}(n_{L_1},n_{L_2},n_{L_3},n_{M_1},n_{M_2},n_{M_3},n_{M_4},n_{M_5})}, \tag{A4}$$

where Γ^k denotes the rate of transition k. Superscripts tot(X) and tot(A) stand for all x-ray and Auger transitions from the given initial state, respectively.

Individual Auger rates $\Gamma_A^0(2p,l_a,l_b)$ for transitions filling a $2p$ vacancy and producing vacancies in the orbitals l_a and l_b were taken from the tables of Walters and Bhalla [15], while the tables of McGuire [16] were used to obtain the total Auger rates $\Gamma_A^0(2s,X_1,X_2)$ and $\Gamma_A^0(2p,X_1,X_2)$, where X_1 and X_2 each denote the shells containing the active electrons. The individual Auger rates for transitions into the $2s$ orbital were obtained using the formula

$$\Gamma_A^0(2s,l_a,l_b)=\Gamma_A^0(2p,l_a,l_b)\times\Gamma_A^0(2s,X_1,X_2)/\Gamma_A^0(2p,X_1,X_2), \tag{A5}$$

where l_a and l_b each denote one of the subshells in the M shell or above. To convert from the dependence on the orbital angular momentum quantum numbers l to the dependence on the total angular momentum quantum numbers j, the following expression was employed:

$$\Gamma_A^0(j_i,j_a,j_b)=\Gamma_A^0(l_i,l_a,l_b)\times[(2j_a+1)(2j_b+1)]/[4(2l_a+1)(2l_b+1)]. \tag{A6}$$

Finally, the rates that apply to atoms with multiple vacancies were obtained by applying the scaling procedure of Larkins [17]

$$\Gamma_A''(j_i,j_a,j_b)=\Gamma_A^0(j_i,j_a,j_b)\times(2j_i+1-n_i)\times[n_a(n_b-\delta_{a,b})]/[(2j_a+1)(2j_b+1-\delta_{a,b})], \tag{A7}$$

where $\delta_{a,b}$ equals 1 if a and b refer to the same subshell and zero otherwise.

Since all the j-dependent single-vacancy-atom x-ray transition rates needed have been calculated by Scofield [18], it was only necessary to apply the scaling procedure to obtain the rates for atoms with multiple vacancies:

$$\Gamma_x''(j_i,j_f)=\Gamma_x^0(j_i,j_f)\times(2j_i+1-n_i)\times n_f/(2j_f+1). \tag{A8}$$

[1] V. Horvat, R. L. Watson, and R. Parameswaran, Phys. Rev. A **51**, 363 (1995).
[2] V. Horvat, R. L. Watson, and J. M. Blackadar (unpublished).
[3] G. J. Pedrazzini, J. Palinkas, R. L. Watson, D. A. Church, and R. A. Kenefick, Nucl. Instrum. Methods Phys. Res. B **10/11**, 904 (1985).
[4] J. P. Rozet, C. Stéphan, and D. Vernhet, Nucl. Instrum. Methods Phys. Res. B **107**, 67 (1996).
[5] J. F. Ziegler (private communication).
[6] W. H. McMaster, N. K. Del Grande, I. H. Mallet, and J. H. Hubell, Lawrence Livermore National Laboratory Report No. UCRL-50174, Sec. II, Rev. 1 (1969) (unpublished).
[7] R. L. Watson, D. Fry, V. Horvat, and J. M. Blackadar, *Progress in Research, 1995–1996* (Cyclotron Institute, Texas A&M University, College Station, TX, 1966), p. 105.
[8] K. Shima, N. Kuno, M. Yamanouchi, and H. Tawara, At. Data Nucl. Data Tables **51**, 173 (1992).
[9] V. S. Nikolaev and I. S. Dmitriev, Phys. Lett. **28A**, 277 (1968).
[10] R. L. Watson, V. Horvat, and J. M. Blackadar, Phys. Rev. A **55**, 1988 (1997).
[11] J. P. Desclaux, Comput. Phys. Commun. **9**, 31 (1975).
[12] P. Beiersdorfer, S. von Goeler, M. Bitter, E. Hinnov, R. Bell, S. Bernabei, J. Felt, K. W. Hill, R. Hulse, J. Stevens, S. Suckerwer, J. Timberlake, and A. Wouters, Phys. Rev. A **37**, 4153 (1988).
[13] K. Shima, T. Ishikara, and T. Mikumo, Nucl. Instrum. Methods Phys. Res. **200**, 605 (1982).
[14] K. Shima, N. Kuno, and M. Yamanouchi, Phys. Rev. A **40**, 3357 (1989).
[15] D. L. Walters and C. P. Bhalla, Phys. Rev. A **4**, 2164 (1971).
[16] E. J. McGuire, Phys. Rev. A **3**, 587 (1971).
[17] F. P. Larkins, J. Phys. B **4**, L29 (1971).
[18] J. H. Scofield, At. Data Nucl. Data Tables **14**, 121 (1974).